

41th Joint Propulsion Conference, July 10-13, 2005, Tucson, AZ

Modeling of Ion Thruster Beam Neutralization Using a Fully Kinetic ES-PIC Code

Lubos Brieda* and Joseph Wang†

Virginia Polytechnic Institute and State University, Blacksburg, VA, 24061-0203

This paper presents a full particle PIC model for near-thruster plume for single and multiple ion thruster systems. Fully kinetic simulations, where both the ions and electrons are tracked as particles, are performed to understand the electron dynamics in the plume and the ion beam neutralization process. A dimensional scaling approach is developed to properly resolve plasma parameters on the computational mesh. A particle boundary treatment, based on conservation of energy, is used to prevent numerical instability. Results for the thruster cluster and a single thruster are compared to a pre-neutralized beam. Comparison with the polytropic model and the Boltzmann relationship is also made.

I. Introduction

Electric thruster plume has been a subject of extensive studies in recent years. Almost all existing plume models focus on charge-exchange ion interactions with the spacecraft and/or plume contamination. A typical particle-in-cell (PIC) based plume model does not model the detailed physics in the near-thruster region, such as the beam neutralization process and the electron dynamics. Rather, the electron characteristics and the near-thruster plume properties are simplified using several assumptions. A commonly used assumption in almost all existing plume models is to assume that the electron density distribution follows the Boltzmann relationship with user supplied values for the electron temperature and beam potential near the thruster. No simulation models are currently available to investigate the near-thruster plume, and the ion beam neutralization process and the characteristics of the neutralizing electrons are still not well understood.

Understanding of the neutralization process will become even more important for electric thruster clusters that are being considered for future space applications. Such a cluster system may use one neutralizer to neutralize ion beams emitted from multiple thrusters. Already, several cluster configurations were tested experimentally by Beal and Hargus.^{1,2} However, experimental measurements can provide only a limited amount of information on the motion of the electrons. The effectiveness of beam neutralization by a shared neutralizer is still not clear, and there is no generally agreed optimal configuration for electric thruster clusters.

This paper presents initial work performed at Virginia Tech's capLAB to model ion beam neutralization. Both electrons and ions were tracked using a macro-particle approach. This formulation avoids solution of the electron fluid equations, which are dependant on a number of coefficients, values of which may not be readily available at the beginning of the simulation. However, the fully-kinetic approach also introduces several new issues in numerical modeling. These issues will also be discussed in this paper. Following section briefly describes the simulation algorithm. Then, a new method for electron modeling using a dimensional scaling and energy particle boundaries is introduced. This method is consequently used to model neutralization of a 40cm ion thruster, operating in a single and a cluster configuration.

II. DRACO ES-PIC Code

A 3D plasma simulation module, called DRACO, is being developed within the AFRL COLISEUM framework. COLISEUM is a collection of modules capable of resolving dynamics of electric thruster plumes,

*Graduate Student, Department of Aerospace and Ocean Engineering, Student Member AIAA, lbrieda@yahoo.com

†Associate Professor, Department of Aerospace and Ocean Engineering, Associate Fellow AIAA, jowang@vt.edu

Copyright © 2005 by the American Institute of Aeronautics and Astronautics, Inc. All rights reserved.

and their interactions with spacecraft surfaces.⁴

The DRACO module tracks particles on a Cartesian mesh, which has been overlaid with a secondary tetrahedral mesh.⁵ This secondary mesh allows DRACO to resolve surface geometries with detail beyond the standard "stair-case" representation attained on Cartesian grids. Surface definition is specified using planar cuts of *interface* tetrahedrons.

The main COLISEUM package contains support for loading of triangular meshes from input files using standard formats such as Ansys or Abaqus. The interface mesh is generated automatically by DRACO's helper module called VOLCAR. The actual intersection process is described in a greater detail elsewhere.⁶

The interface cuts are used to perform particle surface interactions, and, depending on the chosen solver, to obtain the plasma potential, ϕ . The plasma potential is computed from the Poisson's equation,

$$\nabla^2 \phi = -\frac{\rho}{\varepsilon_0} \quad (1)$$

using the DADI⁷ scheme. In the above equation, ρ is the charge density of the particles, C/m³, and ε_0 is the permittivity of free space, 8.854×10^{-12} F/m. The charge density is computed from the individual contributions of the ions and the electrons, $\rho = q(n_i - n_e)$, where $n_{i,e}$ is the number density of the ions or electrons. In the Particle-In-Cell (PIC) method,⁸ the number density is obtained by coupling the particles with the grid through particle *shape factors*,

$$n_k = \sum_i w_i S(x_i - x_k) \quad (2)$$

where x_k is the position of a grid node, and w_i is the specific weight of the macroparticle. In this work, the shape and size of the particles was identical to the Cartesian cell. This first-order representation reduces the simulation noise associated with the zeroeth-order (point particle) model, while still allowing a simple particle-mesh weighing algorithm. The electric field, \vec{E} , is then computed from

$$\nabla \phi = -\vec{E} \quad (3)$$

using the standard centered finite-difference method. Particle velocity is adjusted according to the Lorentz force,

$$m \frac{\partial \vec{v}}{\partial t} = \vec{F} = q \left(\vec{E} + \vec{v} \times \vec{B} \right) \quad (4)$$

where m = particle mass, kg
 \vec{v} = particle velocity, m/s
 q = particle charge, C
 \vec{E} = electric field, V/m
 \vec{B} = magnetic field, T

The electro-static (ES) formulation, implemented by DRACO, assumes that $\partial \vec{B} / \partial t = 0$. No static background field was used in the current simulation, and hence the force acting on the particles was simply

$$m \frac{\partial \vec{v}}{\partial t} = \vec{F} = q \vec{E} \quad (5)$$

The equation of motion for the particles is

$$\frac{\partial \vec{x}}{\partial t} = \vec{v} \quad (6)$$

This equation is integrated numerically along with eq. 5 using the *leapfrog* method with a finite timestep Δt . Final position of the particles is checked for surface interactions. Particles leaving the simulation domain are either removed from the simulation, or are reintroduced according to prescribed boundary conditions. New particles are introduced by sampling particle sources. This process repeats until a user specified condition, such as reaching a steady-state, or exceeding a maximum number of timesteps, is satisfied.

III. Neutralization Modeling

A. Simulation Setup

The ion thruster used in this study was based on the 40cm NASA Evolutionary Xenon Thruster (NEXT). Surface definition of the thruster is shown in figure 1. This mesh was generated using MSC.Patran. It should be noted that a dimensional drawing of the thruster was not available to the authors, and hence the thruster geometry was generated by collecting data from several relevant papers.^{9,10}

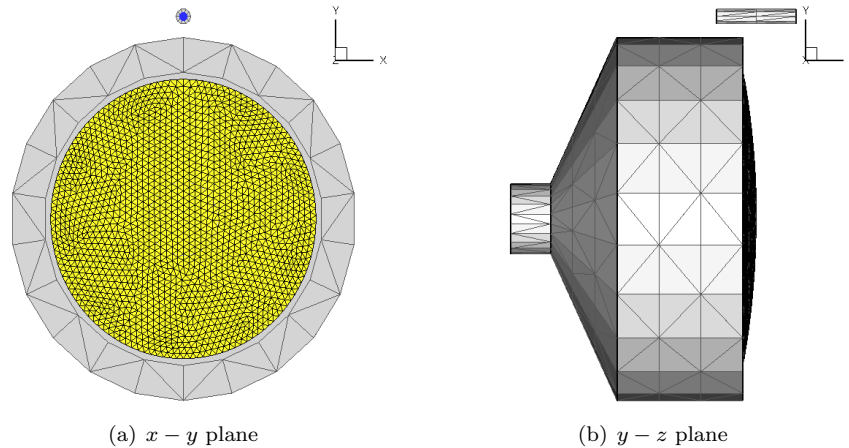


Figure 1. Surface mesh of the ion thruster. The physical curvature of the ion optics was used to introduce curvature to the ion beam. Yellow regions indicates source triangles emitting ions. Electrons are injected from the small blue region at the tip of the cathode.

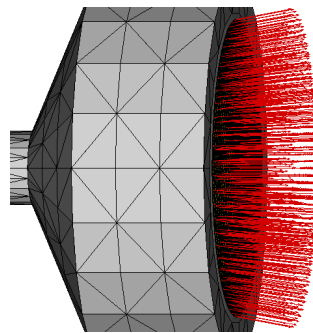


Figure 2. Normal vectors of the particle source elements. These vectors roughly indicate the initial divergence of the ion beam.

COLISEUM particle sources are specified by associating a production model with a collection of surface triangles. Generally, particles are introduced relative to the normal vector of the source triangle. Hence, physical curvature of the surface mesh results in a divergence of the ion beam. This concept is illustrated in figure 2, which shows the normal vectors of the source surface elements. Curvature of the surface mesh resulted in approximately a 15% divergence of the beam. Beam flatness (ratio of current density between the centerline and the edge) was adjusted by biasing the mass production rate of the source elements, according to measurements of Soulas.¹¹ Thruster was assumed to produce 1.2A of beam current, with ions injected with 0.1eV temperature and velocity of 34,400m/s (3510s ISP).¹²

This paper presents preliminary work, which is based on several assumptions:

- The ion plume is composed only of electrons and single charged ions. No neutrals or doubly charge ions were used in the study.
- Collision do not play a significant role. The mean free path for electron-ion collisions in a plasma of density $\sim 10^{15} \text{ m}^{-3}$ and electron velocities $\sim 10^5 \text{ m/s}$ is of $O(0.1)\text{m}$. This distance is similar to

the characteristic dimension of the domain. An electron is hence expected to undergo only several collisions.

- The thruster acts a perfect conductor. Any electrons hitting the thruster were re-emitted from the cathode at the next time step.
- The cathode serves only as a source of electrons, which then flow into the beam. The potential on the cathode was allowed to float. This step was necessary, since the code was not able to correctly resolve the large density difference between the plume and the cathode tip.

B. Dimensional Scaling

The neutralization process can be divided into several regions to simplify the modeling approach. First, a high electron density region exists near the tip of the neutralizing cathode. These electrons flow into the ion beam through a *plasma bridge*. A mixing region is expected to exist at the plane of the cathode. However, beyond this plane, the beam is expected to be relatively well neutralized, and the electrons should travel with the ions.

The neutralized region beyond the plane of the cathode was modeled first. Beam pre-neutralization was approximated by emitting both ions and electrons from the thruster optics. This approach allowed us to study the numerical approach needed to model electrons without the secondary influence of electron flow from the external cathode. Among other things, it allowed to determine whether DRACO was actually capable of resolving the containment of electrons in the ion beam.

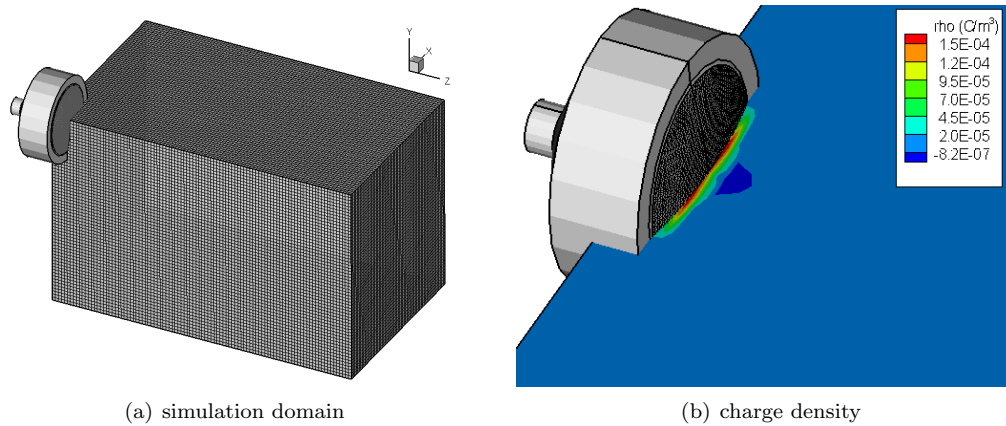


Figure 3. Initial simulation domain and charge density after 30,000 time steps. Uniform simulation cell size of 2cm was used, resulting in a formation of a virtual anode.

Figure 3(a) shows the simulation setup. Due to symmetry, only a quarter domain was simulated. However, retaining a numerically sound number of computational nodes ($\sim 10^6$), required use of cells with length of 2cm, or approximately $100\lambda_D$, where λ_D is the Debye length.

The PIC formulation replaces point sized particles with particles with the size of the cell. Hence, no detail is available on length scales smaller than the cell size. Furthermore, λ_D specifies the approximate distance at which quasi-neutrality can be assumed. Motion of the electrons is influenced by electric field which arises due to local charge non-neutralities. Simulation cell many orders of magnitude larger than the Debye length is not capable of resolving these charge variations. Influence of this limitation is clearly visible in figure 3(b). This figure shows the simulation result after approximately 30,000 simulation time steps, in which Δt was adjusted automatically, according to the CFL condition. Instead of a distinct ion beam, the simulation develops a solution typical of a virtual anode.¹³

Obvious step would be to reduce the cell size to approximately λ_D . However, retaining the physical span would require a million-fold increase in number of mesh nodes. Not only would such a mesh be difficult to store in memory, it would also drastically increase the computational time needed to solve the Poisson's equation. Hence, another approach had to be taken.

Using an artificially high electron mass would destroy the meso-thermal relationship existing between the ions and the electrons. Instead, the simulations presented here were performed with *scaled-down* thrusters.

The thruster dimensions were reduced by a factor of 100. This reduction required an adjustment to the thruster operating conditions to preserve the plasma environment through scaling. Beam current was reduced by a factor of 10,000 (100^2), which retained the plasma density at the thruster exit. A somewhat more detailed treatment of scaling is available in Ref. [6].

C. Results with Open Boundaries

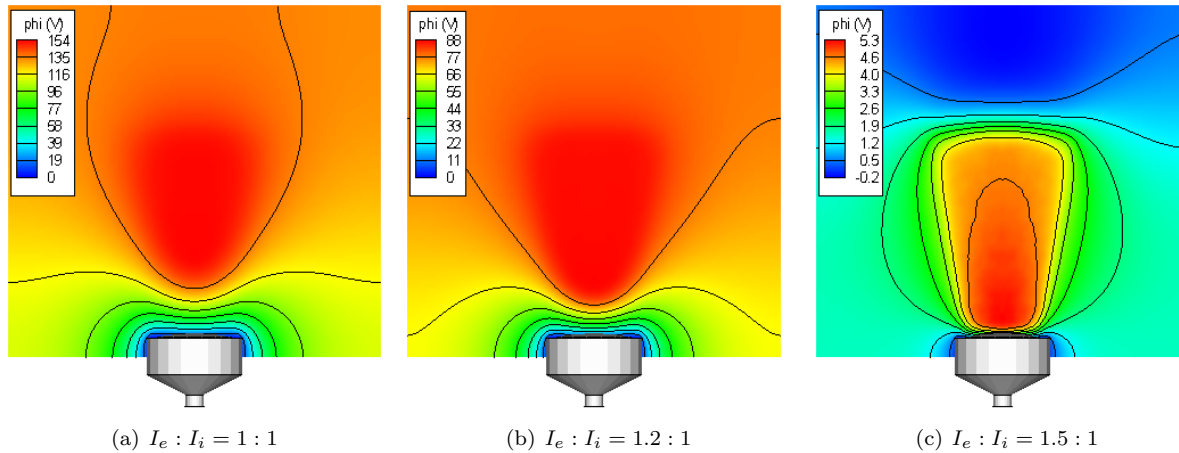


Figure 4. Potential after 3×10^{-7} seconds, open boundary conditions. Electrons were injected from the ion optics.

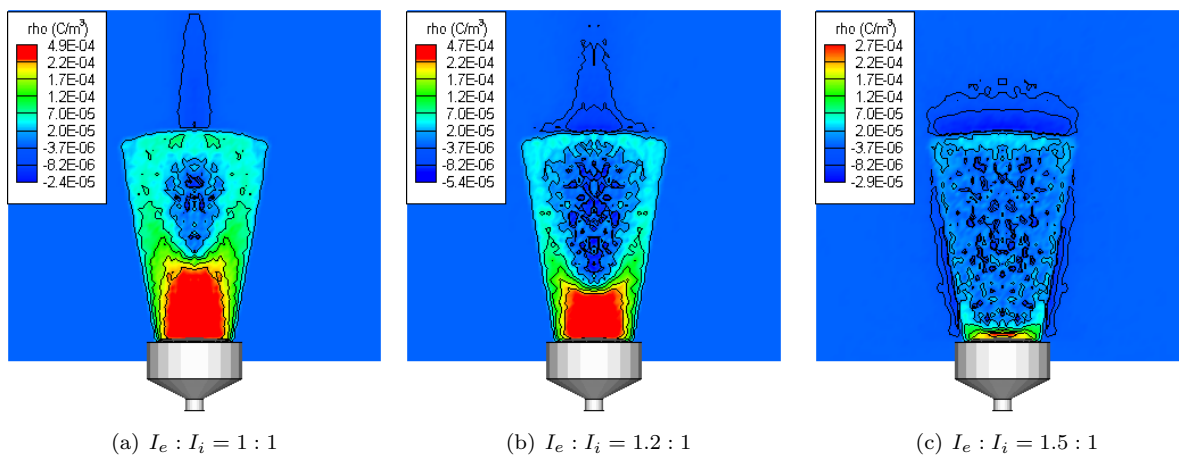


Figure 5. Charge density after 3×10^{-7} seconds, open boundary conditions. Electrons were injected from the ion optics.

The scaled down thruster was used to study the effect of electron-to-ion beam current on the plume parameters. Three $I_e : I_i$ ratios are presented here: 1:1, 1.2:1, and 1.5:1. Simulations ran for 3×10^{-7} plasma seconds, which corresponded to about 4,500 time steps for the first case, and 2,500 time steps for the last one. Of course, the physically accurate ratio is 1:1, however, as can be seen from the series of plots in figure 4 through 6, this case develops a very high beam potential, a non-neutral beam, and a distinct high temperature region near the potential hill. Increase in electron current lowered the beam potential, but a distinct beam structure does not develop until electron current is increased to $1.5I_i$. On the other hand, the third case, in which $I_e : I_i = 1.5 : 1$, produces physically sound results, with maximum beam potential of 5.3V, and maximum electron temperature of 2.8eV. Furthermore, the temperature is seen to decrease with beam divergence, which was not true in the first configuration.

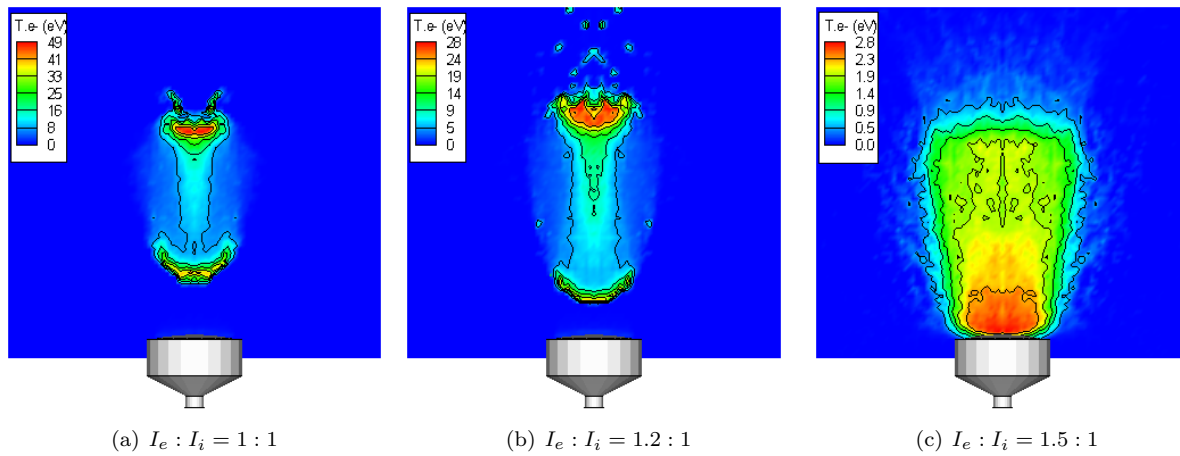


Figure 6. Electron temperature after 3×10^{-7} seconds, open boundary conditions. Electrons were injected from the ion optics.

D. Numerical Pump Instability

High potential for the 1:1 case is due to a lack of sufficient number of electrons to neutralize the beam. Since an equal electron and ion currents are being injected, the lack of electrons must be associated with a “leakage” of electrons through the boundaries of the simulation domain. Above simulations used open external boundaries, and hence all particles leaving the domain were simply removed from the simulation. Interesting is the presence of an electron *jet* in figures 5(a) and 5(b). This jet is absent in 5(c). This case instead develops what seems to be an electron sheath surrounding the beam.

The electron jet indicates a region of highly focused electrons leaving the domain. A more detailed analysis⁶ indicated that the jet forms after background electrons start leaving the simulation domain due to their random walk. Removal of electrons at the boundaries results in $\rho_{nz-1} < \rho_{nz}$, where ρ_{nz} is the charge density at the last mesh node. Since the second-to-last cell contains more electrons than the last cell, a small electric field develops, directing electrons into the last cell. The electrons however overshoot the last cell because of their inertia. Hence, instead of equalizing the charge density, the electric field results in an increased removal of electrons. This cascading effect demonstrates itself as the highly focused electron jet. This instability acts in a fashion similar to a vacuum pump operating outside the boundaries of the simulation domain, by “sucking-out” electrons from the beam.

E. Energy Boundary Condition

A new particle boundary model had to be developed to reduce the removal of electrons at the boundaries. Several options were investigated, including *thermalization* of electrons. Since the instability is due to removal of randomly-moving background electrons, the electrons could be re-introduced back to the domain with a new random velocity, based on a user specified “wall” temperature. However, since a perfect-conduction model was employed on the thruster, use of thermal boundaries on all external faces would result in an absence of particle sinks in the domain. The beam is capable of “shedding” extra electrons, due to their high mobility. Without available particle sinks, these extra electrons would not be able to leave the domain.

The external boundary had to act as a filter, allowing some electrons to leave the domain, while retaining those which should be contained by the beam. Conservation of energy requires that

$$\frac{1}{2}m_e v_e^2 - e\Delta\phi = E_0 \quad (7)$$

where E_0 is a constant. Let’s assume that a particle is introduced with zero velocity at the bottom of a potential hill. This situation is sketched in fig. 7. As the particle starts traveling up the hill, it begins to trade its initial potential energy for kinetic energy. The kinetic energy (velocity) reaches a maximum value at the top of the hill. The flow of energy reverses as the particle continues past the peak and the electron comes to a stop after traveling down the initial $\Delta\phi$. The particle cannot continue any further, since that would require a negative KE. The electron will instead start traveling up the hill; it is trapped in the potential hill.

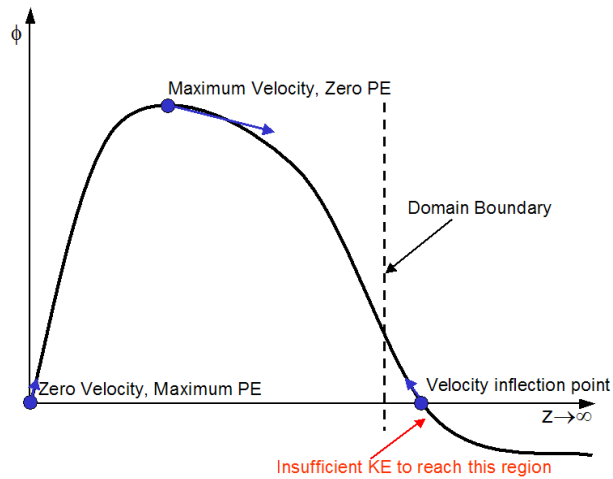


Figure 7. Conservation of energy in electron dynamics. Placing the domain boundary before the electron velocity inflection point results in a loss of electrons which are trapped in the potential hill.

Due to finite domain dimensions, the inflection point may be located outside the simulation domain. Electrons which should remain trapped in the beam are removed by the open boundary. The newly developed energy particle boundary uses conservation of energy to reflect the trapped particles. This model assumes that all electrons start from rest, and travel through the region of maximum potential. Furthermore, the particles are reflected immediately, even though some time is needed for the particle to travel to the inflection point and back. The effect of these approximations on simulation results needs to be studied further.

F. Cathode Model

The diameter of the cathode orifice was assumed to be 1.2cm. The injection area of the electrons is hence 5 orders of magnitude smaller than the injection area of the ions. Approximating electron velocity as 5×10^5 m/s, and using injection ion velocity of $\sim 30,000$ m/s, the ratio of electron to ion densities at the source is

$$\begin{aligned} \frac{n_e}{n_i} &= \frac{I}{A_e v_e} \frac{A_i v_i}{I} \\ \frac{n_e}{n_i} &= \frac{A_i v_i}{A_e v_e} \\ \frac{n_e}{n_i} &\sim 100 \end{aligned} \quad (8)$$

Since the Debye length scales as $\sqrt{1/n}$, the cell size near the cathode tip should be about 30 times smaller than the cell size used to resolve the beam dynamics. Although DRACO contains a rudimentary support for mesh refinement, additional work is needed to assure continuity of the potential solution across mesh boundaries. Furthermore, the current implementation can resolve only a 1:2 refinement, and thus at least 5 mesh levels ($2^5 = 32$) would be needed to correctly resolve λ_D .

Instead, a simplified cathode model has been developed. Since the simulation was not greatly concerned with the plasma properties near the cathode tip, the cathode was used only to introduce electrons at an appropriate distance from the beam. Two approximations were made. First, the charge density around the cathode was limited to $\sim -2.7 \times 10^{-4}$ C/m³. However, even with this limiting value, a large non-physical potential gradient developed between the cathode edge and the electron dominated region. This gradient introduced a great velocity boost to the electrons, which then escaped without being able to turn into the beam. Hence, the potential on the cathode was allowed to float. This approximation resulted in the electrons turning into the beam, at the added accuracy cost of variable $\Delta\phi$ between the cathode and the beam.

IV. Results

A. Overview

The dimensional-scaling approach with energy boundaries was used to model neutralization in three thruster configurations. These configurations were compared to the reference pre-neutralized case (case R2), in which both the electrons and ions were injected from the optics. The studied cases included:

- Case NS: single thruster
- Case NI: 2x2 cluster with individual cathodes
- Case NC: 2x2 cluster with a single central cathode

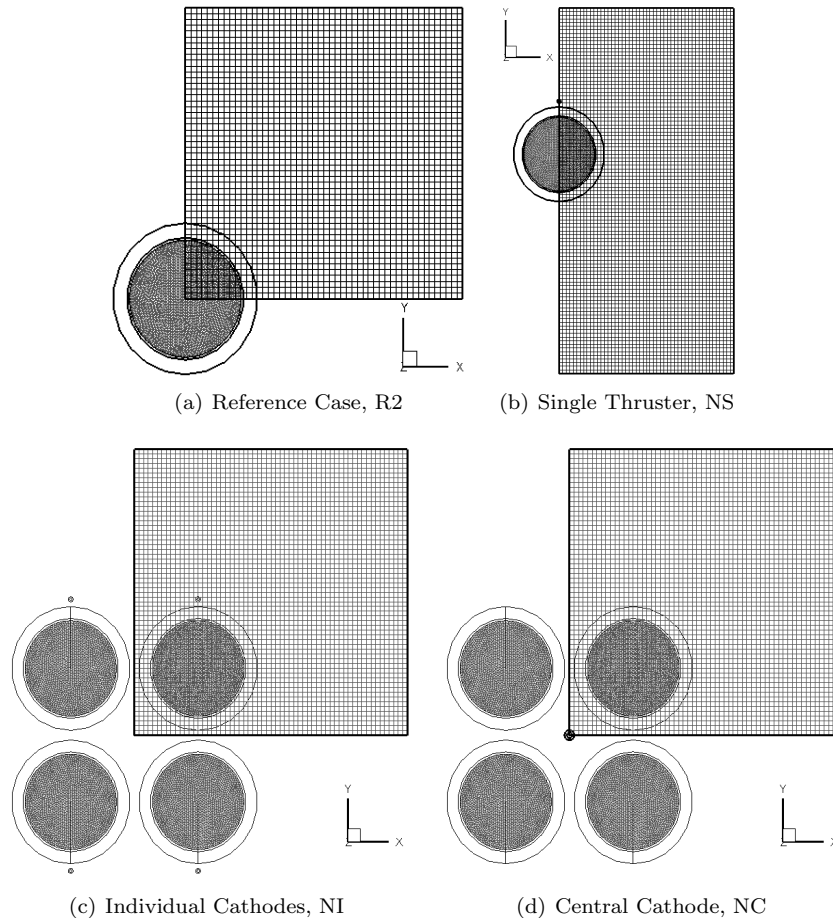


Figure 8. Simulation domain for neutralization configurations. Only minimum domain was simulated, due to symmetry. Uniform cell spacing of 2×10^{-4} m was used in all cases.

Figure set 8 shows the $x - y$ plane of the simulation domain for the studied cases. In all cases, only the minimum domain was simulated. A reflective particle boundary condition was used along the symmetric faces. The grid dimensions varied slightly between the cases; $50 \times 50 \times 90$ nodes were used for R2, $50 \times 100 \times 90$ for N2, and $60 \times 60 \times 90$ for NI and NC. Uniform cell spacing of 2×10^{-4} m was used in all configurations.

B. Reference Case

Simulation results on the symmetry plane for the reference case are shown in figure 9. A distinct beam profile is seen in the plot of the potential. Potential reaches about 4.7V in the core near the thruster exit, and is seen to decrease with beam divergence. Similar observation is made for the electron temperature. The electron temperature was computed assuming Maxwellian distribution. Temperature reaches approximately

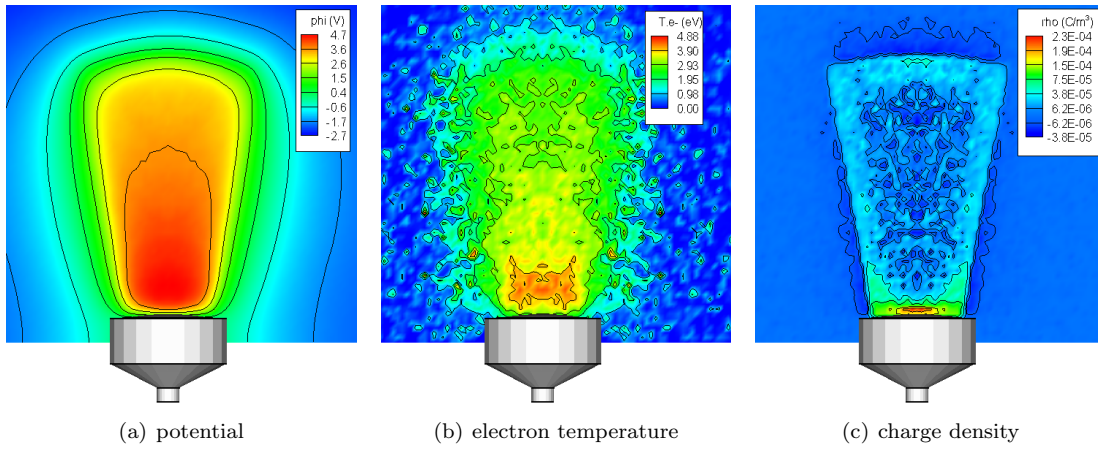


Figure 9. Potential, electron temperature, and charge density after 3×10^{-7} seconds, for a single thruster.

5eV near the thruster exit. Last plot shows the charge density, $\rho = q(n_i - n_e)$. Good neutralization is indicated by light-blue shading. The charge density in the beam is seen to be slightly positive, which leads to the positive potential in the beam. An electron sheath is seen to surround the beam. This sheath is responsible for the containment of the electrons in the beam.

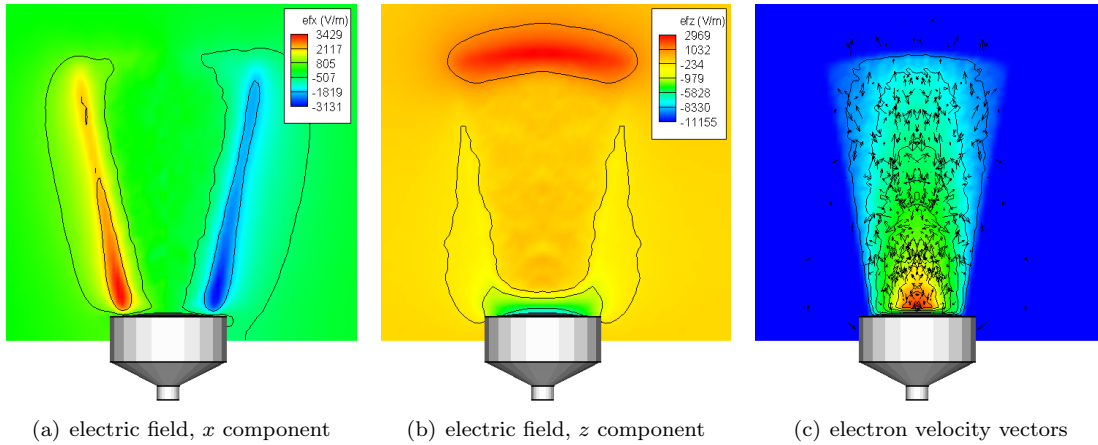


Figure 10. Electric field and electron velocity vectors for the reference case. Electrons were injected from the optics using Maxwellian distribution with $T_e = 1\text{eV}$.

The electric field components, $\vec{E} = -\nabla\phi$, are shown in figures 10(a) and 10(b). Both the radial and the axial components are seen to be approximately zero in the bulk of the beam. Hence, the acceleration of the electrons is expected to be limited to the regions near the edge of the beam, with electrons moving at constant velocities inside the beam core. The motion of the electrons is highly random (fig. 10(c)), even though they were originally injected in the axial direction, using a Maxwellian source with $T_e = 1\text{eV}$. Due to their high mobility, the electrons seem to have only a weak memory of their injection distributions.

Maxwellian temperature obtained from the simulation is compared to the polytropic relationship

$$T = T_0 \left(\frac{n}{n_0} \right)^{(\gamma-1)} \quad (9)$$

for three values of γ in figure 11(a). Reference temperature and density were chosen to correspond to the values in the beam core, 4.2eV and $2.5 \times 10^{15} \text{ m}^{-3}$, respectively. Neither of the three chosen gamma values was able to produce an exact match, however, the temperature seems to roughly follow the polytropic relationship with $\gamma \sim 1.4$.

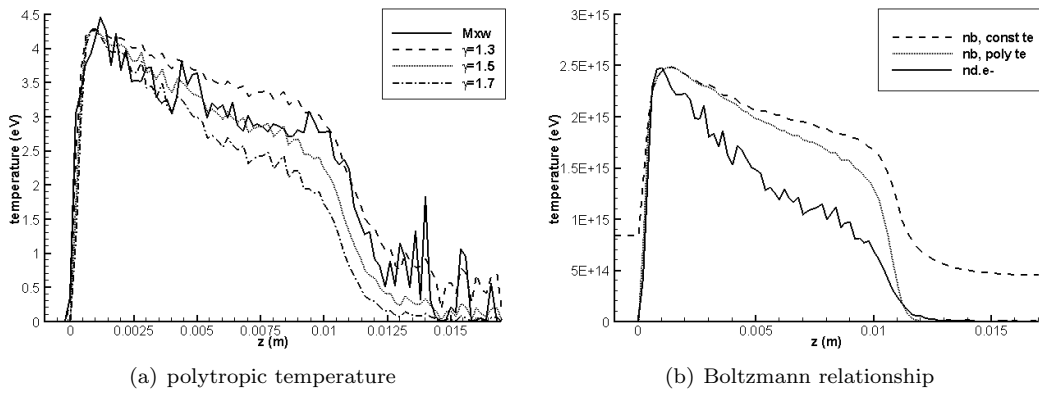


Figure 11. Comparison of numerical temperature to the polytropic model, and comparison of simulation electron density to prediction using Boltzmann model.

Numerical electron density was also compared against the Boltzmann relationship. It states that a direct relationship exists between plasma potential and plasma density,

$$n_e = n_0 \exp\left(\frac{\phi - \phi_0}{kT_0}\right) \quad (10)$$

Again, plasma properties in the beam core were used for the reference values. Reference potential was set to 4.7V. The relationship was computed using both constant reference temperature (4.2eV), and polytropic temperature with $\gamma = 1.4$. Generally, the agreement is not very good, as figure 11(b) shows. Best agreement is achieved near the core, which is expected, since this location corresponds to the point at which the reference values were sampled. The simulation electron density drops off faster than predicted by the model. The disagreement is reduced by using the polytropic temperature, however, a significant discrepancy still remains. A better agreement could be achieved by adjusting the reference parameters; this approach however requires prior knowledge of the solution.

C. Single Thruster

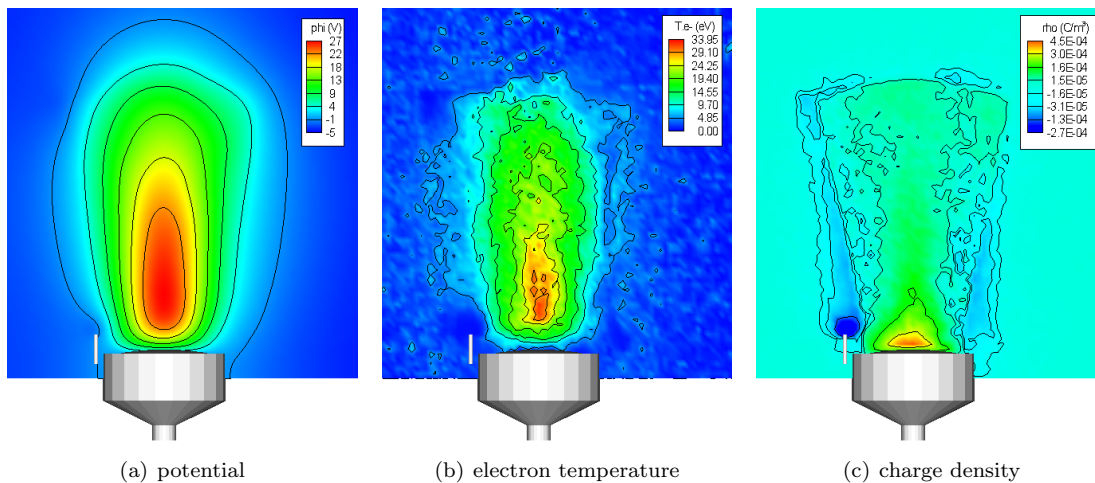


Figure 12. Potential, electron temperature, and charge density after 3×10^{-7} seconds, for a single thruster.

The simplified cathode model, described in the previous section, was used next to model neutralization of a single thruster. Obtained results on the cathode plane (plane of symmetry) are shown in figure strip 12. Results were expected to agree with the pre-neutralized case R2, but a quick comparison with figure 9 shows a noticeable amount of divergence. The beam shape is no longer well resolved. Furthermore, the potential

in the core of the beam increased to 27V. Maximum electron temperature also increased to 34eV. Average beam temperature is approximately 15eV.

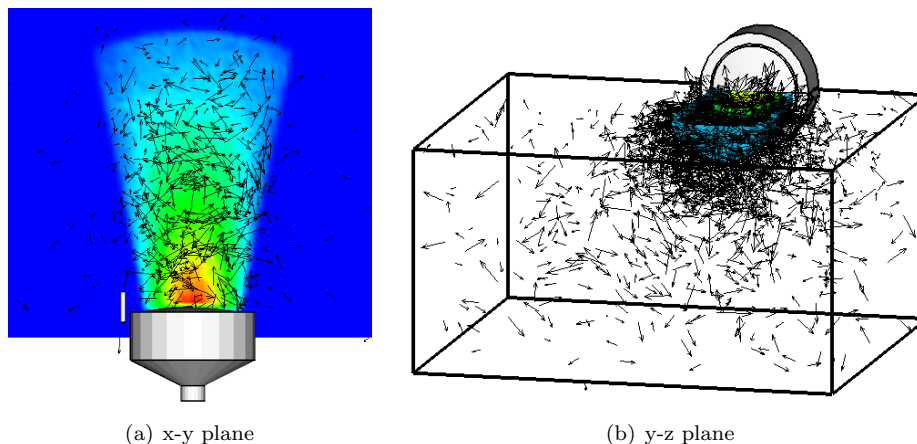


Figure 13. Electron velocity vectors for single-thruster neutralization.

These results indicate a problem in the neutralization modeling, which leads to a worse beam neutralization. The cause has not yet been discovered, but the difference could be due to the simplifying assumptions made in cathode modeling. Yet, the cathode electrons are seen to flow into the beam, and an electron sheath structure does develop. However, the sheath is not as well defined as it was in the R2 case, perhaps suggesting that the beam is lacking sufficient number of electrons. Since injection $I_e = I_i$, lack of electrons indicates escape of particles through the energy boundaries. This possibility was tested by over-saturating the central cathode cluster case (NC1) with electrons. However, even though the injection I_e was set to $1.5I_i$, that configuration (NC2) did not show a significant improvement in the beam profile.

Time snapshots of simulation results indicate that the electrons emitted from the cathode initially overshoot the beam. It is possible that coupling of this overshoot with the elastic reflection at the energy boundary introduces fluctuations into the solution. Similar fluctuation could arise from the time-varying potential on the cathode. These possibilities were not examined in this simulation, and remain to be studied further. Electron velocity vectors are plotted in figure 13. Once again, the motion of the electrons is very random. No direct correlation between cathode placement and the electron motion is observed.

D. Cluster with Individual Cathodes

A 2x2 cluster configuration was studied next. Each thruster was neutralized using an individual cathode. Results for this configuration are shown in strip 14 and show similar problems noticed in the single-thruster case. Beam parameters are plotted on the cathode plane, which was extracted by joining the center of the cathode with the center of the thruster. Hence, the cuts do not slice through the center of the cluster. This cut was chosen since it demonstrated more interesting dynamics than the diagonal cut. Results along the diagonal cut are available in [6].

The potential contour clearly shows the effect of beam focusing in the region where the individual beams start to overlap. The potential in the core is approximately equal to the NS case, however, the potential in the electron dominated background region dropped to -16V. Interesting is the clear departure of temperature from the polytropic relationship of the previous cases. Not only does the region of maximum temperature differ from the region of maximum beam density, the temperature profile show a distinct streak of cold (i.e. focused) electrons. This streak originates at the cathode and continues to the plane of symmetry. A clear reflection is visible. A reflection along a symmetric plane simply indicates a flow of electrons from the *neighboring* thruster. The streak disperses near the beam edge. Hence, it seems that in this 2x2 cluster configuration, each thruster is neutralized (at least partially) by electrons from a neighbor thruster.

E. Cluster with a Central Cathode

The individual cathodes were replaced by a single central neutralizer. The injection current was increased to 4.8A ($4I_i$). To retain electron density at the cathode tip, the injection area was increased by a factor of

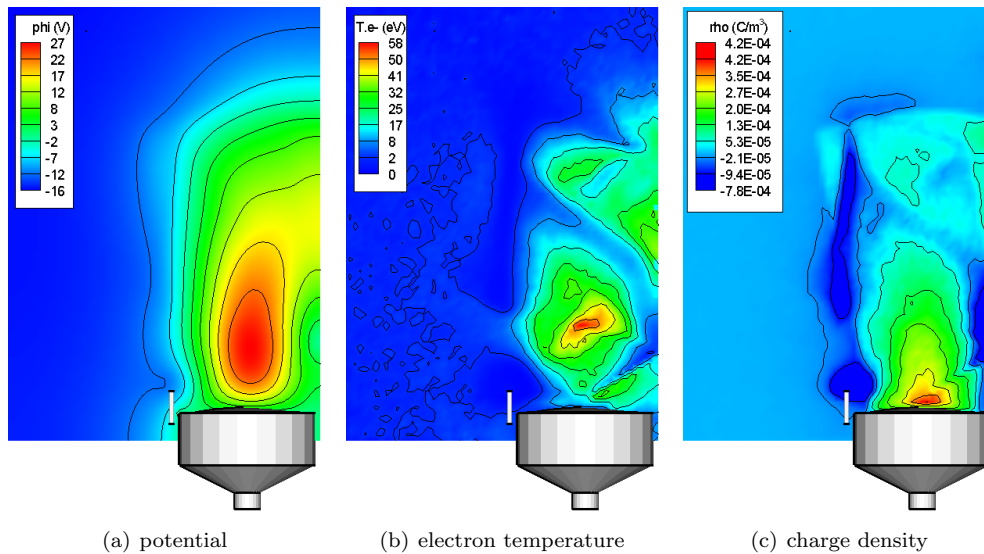


Figure 14. Potential, electron temperature, and charge density after 3×10^{-7} seconds, for a cluster with individual cathodes. Plots are shown on the cathode plane.

4. Results for this case after 3×10^{-7} plasma seconds on the diagonal plane are shown in figure 15.

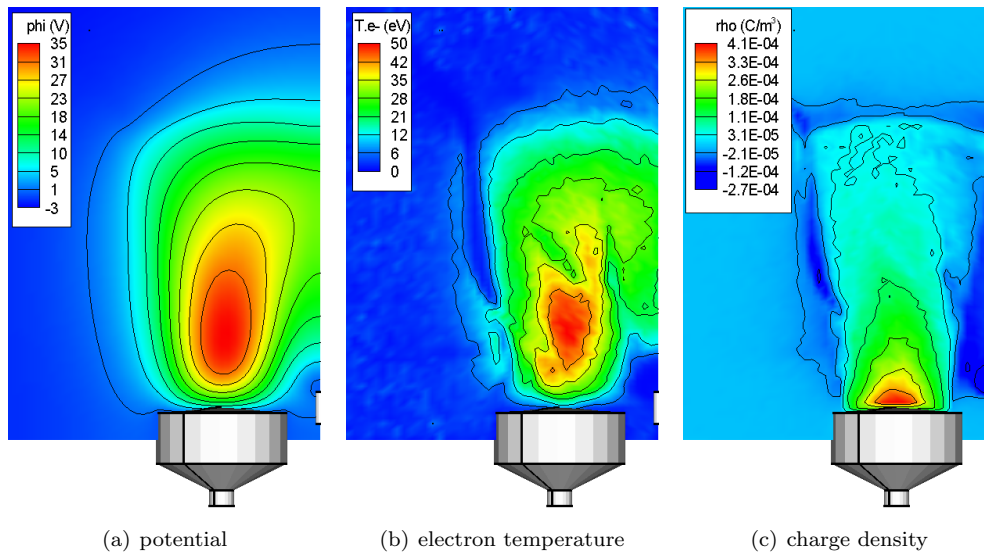


Figure 15. Potential, electron temperature, and charge density for a cluster with single neutralizer, case NC1

This configuration shows a somewhat better agreement with the reference case. Although the peak potential increased to 35V, the total $\Delta\phi$ between the core and the ambient plasma is lower than in case NI. Furthermore, electron temperature shows a closer relationship to the beam density. Yet, the temperature profile is not smooth, and several regions indicative of a rotational motion can be seen. The electron sheath, shown in the charge density plot, is also better developed than in case NI.

As was mentioned previously, effect of electron leakage through the domain boundaries was tested by over-saturating the beam with the electrons. This was achieved by injecting 1.5 times greater electron current from the central cathode. Results for this case (NC2) can be seen in fig. 16. The most noticeable result is the increased beam focusing due an increase in negative charge density at the cluster centerline. However, the beam potential remains large, and the electron temperature is clearly non-polytropic. Hence, the discrepancy of results between the reference R2 case, and the subsequent cases in which electrons were injected from the cathode, does not seem to be due to a lack of neutralizing electrons.

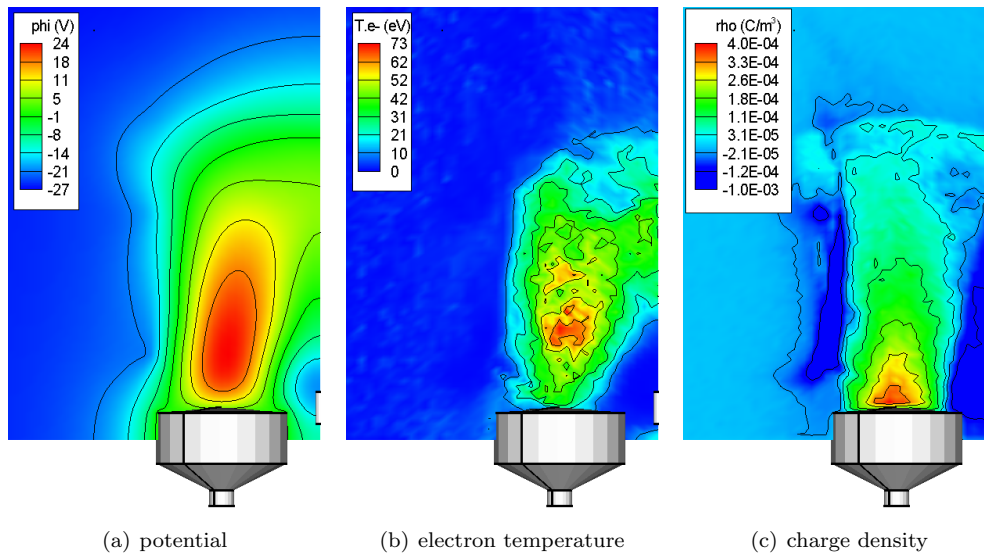


Figure 16. Potential, electron temperature and charge density for a cluster with single neutralizer, and increased electron current, case NC2

F. Velocity Profiles

Final particle velocities were sampled to obtain velocity histograms for the two species. These plots are shown in figure 17. The ion profile for the pre-neutralized case closely follows the Maxwellian distribution. Lack of good neutralization in the cathode cases however results in a departure from the Maxwellian, and the mean drifting velocity of the ions is seen to decrease. The ions are starting to slow down, since they have to cross a higher beam core potential.

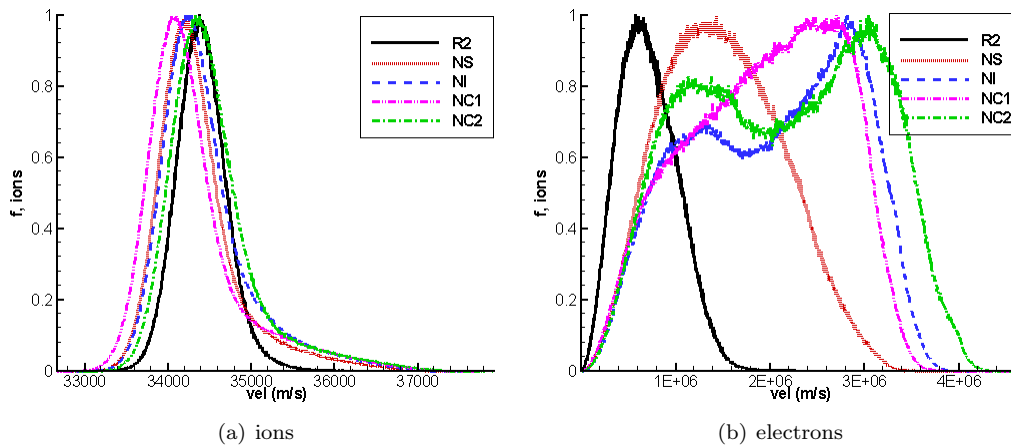


Figure 17. Ion and electron velocity distribution at the end of simulation.

The electron profile shows an even greater discrepancy. The distribution for the single thruster shows the greatest agreement with the reference R2 case. However, the temperature is seen to increase, which is demonstrated by the widening of the distribution function. The mean drift velocity also increases to about 1.8×10^6 m/s. The next closest match is achieved in the cluster configuration with a single neutralizer. Interesting is the development of a secondary hump in case NI. These two electron families could be associated with mixing of the electrons from neighboring thrusters. The over-neutralized case, NC2, also develops a similar profile.

V. Conclusion

A new simulation model for study of ion-beam neutralization was developed. This model uses a fully-kinetic formulation, in which both electrons and ions are tracked as macro-particles. This formulation avoids problems associated with fluid modeling of the electrons, but introduces numerical difficulties. Specifically, it was found that correct modeling of the electron motion depends on the resolution of the local Debye length. A computationally excessive number of nodes would be required to resolve the Debye length on the full-scale geometry. Hence, a dimensional scaling approach was developed.

Dimensional scaling correctly resolved the initial electron motion, but a secondary pump instability developed. Origin of this instability was traced to a removal of randomly-moving background electrons at the domain boundaries. A new particle boundary condition, based on conservation of energy, was developed to overcome the instability. This simulation approach was then applied to modeling of the beam neutralization in the NASA NEXT ion thruster. A reference case was setup by injecting both the electrons and ions from the optics. The potential solution for this case showed a clear beam profile, with maximum value of 4.7V. The electron temperature reached about 5eV in the core, and decreased with density decrease. Comparison to with the polytropic model showed a good agreement for $\gamma \sim 1.4$. The electron density was also compared to the Boltzmann model, but the two plots diverged for the chosen coefficients.

Neutralization of a thruster using an external cathode was studied next, for single thruster and cluster configurations. A significant divergence between the cathode runs and the pre-neutralized case was observed. Injection of electrons from the cathode resulted in a worse neutralization, which demonstrated itself in a higher beam potential, and a departure of the temperature from the polytropic model. The discrepancy does not seem to be due to a lack of neutralizing electrons. Effect of other factors remains to be studied.

Acknowledgments

Authors would like to thank the Air Force Research Laboratory at Edwards AFB for financial support in development of the DRACO code. Additional thanks goes to Chris Hoffman and Preston Geren from the Boeing Company for introducing the first author to neutralization modeling. Access to a large number of computational stations was made thanks to an excellent work of VT AOE department's system administrator Luke Scharf.

References

- ¹Beal, B., Gallimore, A., Haas, J., and Hargus, W., "Plasma Properties in the Plume of a Hall Thruster Cluster," *Journal of Propulsion and Power*, Vol. 20, No. 6, 2004
- ²Hargus, W., Cappelli, M., "Interactions Within a Cluster of Low Power Hall Thrusters," *AIAA/ASME/SAE/ASEE Joint Propulsion Conference and Exhibit*, 39th, Huntsville, AL, July 20-23, 2003.
- ³Hargus, W., Cappelli, M., "Interior and Exterior Laser-Induced Fluorescence and Plasma Measurements within a Hall Thruster," *Journal of Propulsion and Power*, Vol. 18, No. 1, 2002
- ⁴Gibbons, M., Kirtley, D., VanGilder, D., and Fife, J., "Flexible Three-Dimensional Modeling of Electric Thrusters in Vacuum Chambers," AIAA-2003-4872, 2003
- ⁵Brieda, L., Pierru, J., Kafafy, R., and Wang, J., "Development of the DRACO Code for Modeling Electric Propulsion Plume Interactions," *AIAA/ASME/SAE/ASEE Joint Propulsion Conference and Exhibit*, 40th, Fort Lauderdale, FL, July 11-14, 2004.
- ⁶Brieda, L., "Development of the DRACO ES-PIC Code and Fully-Kinetic Simulation of Ion Beam Neutralization", Master's Thesis, Aerospace and Ocean Eng. Dept., Virginia Tech, Blacksburg, VA, 2005
- ⁷Hewett, D., Larson, W., and Doss, S., "Solution of Simultaneous Partial Differential Equations Using Dynamic ADI: Solution of the Streamline Darwin Field Equations," *Journal of Computational Physics*, Vol. 101, 1992, pp. 11-24
- ⁸Birdsall, C., and Langdon, A., *Plasma Physics Via Computer Simulations*, Institute of Physics Publishing, Philadelphia, 2000
- ⁹Patterson, M., et. al, "NEXT: NASA's Evolutionary Xenon Thruster," *AIAA/ASME/SAE/ASEE Joint Propulsion Conference and Exhibit*, 38th, Indianapolis, IN, July 7-10, 2002.
- ¹⁰Soulas, G., Dmonkos, M., and Patterson, M., "Performance evaluation of the NEXT ion engine," *AIAA/ASME/SAE/ASEE Joint Propulsion Conference and Exhibit*, 39th, Huntsville, AL, July 20-23, 2003
- ¹¹Soulas, G., Haag, T., and Patterson, M., "Performance evaluation of 40 cm ion optics for the NEXT ion engine," AIAA Paper 2002-3834, July 2002.
- ¹²NASA Glenn Website, *NASA's Evolutionary Xenon Thruster (NEXT)*, <http://space-power.grc.nasa.gov/ppo/projects/next/accomp.html>
- ¹³Wang, J., and Lai, S., "Virtual Anode in Ion Beam Emission in Space: Numerical Simulations," *Journal of Spacecraft and Rockets*, Vol. 34, No. 6, 1997